Effect of Asymmetric Layout of IGBT Modules on Reliability of Motor Drive Inverters

Ui-Min Choi, *Member, IEEE*, Ionut Vernica, *Member, IEEE*, and Frede Blaabjerg, *Fellow, IEEE*

***Abstract*—Power electronics inverters are one of the major failure sources in motor drive systems, and power devices are one of the main causes of the power electronics inverter failures. Typically, an insulated-gate bipolar transistor (IGBT) module has multiple power devices due to some technical and cost advantages. This kind of configurations could have an asymmetric internal layout, which may lead to different thermal loadings and thereby lifetime difference of the power devices. Therefore, both the power rating and the lifetime of inverters are limited by the most stressed device. However, generally common data are provided for all devices in the datasheet and this may cause improper design of the inverters in terms of the lifetime and the power rating. In this paper, an effect of an asymmetric layout of IGBT modules on the reliability of motor drive inverters is studied based on a three-phase motor drive application with a 600 V, 30 A, three-phase transfer molded IGBT module. The thermal impedances of six IGBTs are investigated and its effect on thermal loadings of power devices is studied under the given mission profile. Then, their lifetimes are estimated and compared. Finally, this effect is verified by the experiments.**

***Index Terms*—insulated-gate bipolar transistor (IGBT) module, inverter, motor drives, reliability.**

I. Introduction

MOTOR drive systems have been widely used in various applications such as ship propulsion, rail traction, steel mills, water pump system, and home appliance, and nowadays their use has been extended to aerospace, electric vehicle, etc. [1], [2]. As roles of motor drive systems have gradually increased, the reliability of motor drive systems is becoming an important issue because it is very closely related to the cost aspect as well as the safety aspect. According to [3], power electronics inverters are one of the major failure sources in motor drive systems, and power devices are one of the main causes of power electronics inverter failures [4]. Therefore, much research has been performed on the reliability of power devices such as condition monitoring, fault detection, and fault-tolerant

Manuscript received November 17, 2017; revised February 13, 2018; accepted April 3, 2018. Date of publication April 17, 2018; date of current version December 7, 2018. This work was supported by Advanced Power Electronic Technology and Tools (APETT) funded by Innovation Fund Denmark. Recommended for publication by Associate Editor J. Rabkowski. *(Corresponding author: Ui-Min Choi.)*

U.-M. Choi is with the Department of Electronic and IT Media Engineering, Seoul National University of Science and Technology, Seoul, Korea (e-mail:

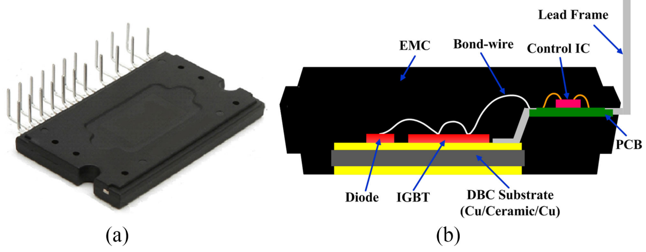

Fig. 1. Transfer molded IGBT module. (a) Physical appearance. (b) Cross-section structure.

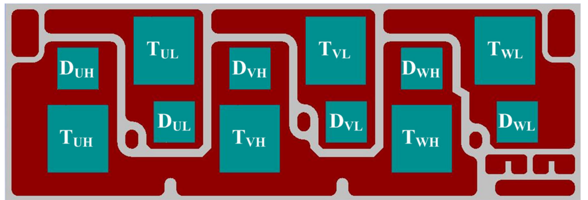

Fig. 2. Internal layout of the molded IGBT module shown in Fig. 1.

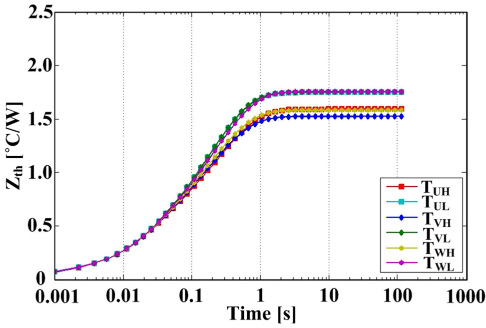

Fig. 3. Transient thermal impedances of the six IGBTs in the molded IGBT modules.

Fig. 1 shows one kind of transfer molded IGBT modules, which is the target IGBT module in this paper. The power rating is 600 V and 30 A and it consists of six IGBTs and six diodes. They are mounted on a direct bonded copper (DBC) substrate with wire-bond interconnection. The lead frame is connected to the DBC substrate by soldering and a copper surface of the DBC substrate is exposed to be contacted with an external heat-sink. Furthermore, gate driver circuits are embedded inside the module.

Fig. 2 shows the internal layout of the target IGBT module. This module has the asymmetric internal layout, especially between the upper group of power devices (IGBTs: $T_{\mathrm{XH}}(X = U, V, W)$ and diodes: D_{XH}) and the lower group of power devices (IGBTs: T_{XL} and diodes: D_{XL}). Thus, it can be expected that they have different thermal impedances in practice.

B. Thermal Impedances of Power Devices in a Molded Power IGBT Module

Fig. 3 shows transient thermal impedances of the six IGBTs obtained by a finite element method simulation. In this module, power losses in the IGBTs are dominant when it is used for inverters, and therefore, this paper is focusing on the IGBTs. Each IGBT has almost the same impedance at a short transient time, which is below 0.05 s. However, the lower group of IGBTs ($T_{\mathrm{UL}}, T_{\mathrm{VL}}, T_{\mathrm{WL}}$) has higher thermal impedances than the upper group of IGBTs (T_{UH}, T_{VH}, T_{WH}), when the transient time is longer than about 0.05 s. Its difference gets larger as the transient time gets longer and is saturated as constant around 2 s. From this, it can be expected that a fast power loss variation by a periodical commutation of the IGBT does not affect the temperature difference among the IGBTs. However, the power loss variation at low fundamental frequencies of output or the power loss variation by load changes, which is typically in the second range or above, leads to different thermal loadings of the IGBTs, and finally, it results in the lifetime difference among the IGBTs.

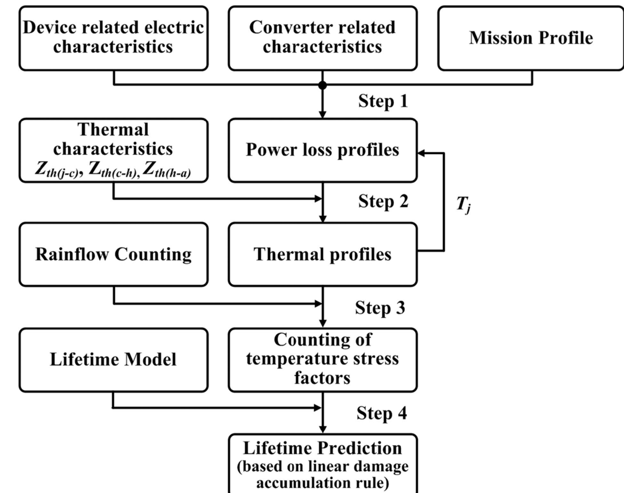

Fig. 4. Lifetime estimation procedure of IGBT modules in power converter applications [17].

III. Lifetime of a Molded Power IGBT Module in a Motor Drive System

In order to investigate the effect of the thermal impedance difference on the reliability of the upper and lower IGBTs, a case study is carried out with a specific mission profile of a motor application. T_{VH} and T_{VL} are considered in this case study because they have the largest thermal impedance mismatch, and the thermal impedances of T_{UL}, T_{VL}, and T_{WL} are almost the same. The thermal loadings of T_{VH} and T_{VL} are investigated and then the lifetimes are estimated based on their thermal loadings.

Fig. 4 shows the whole procedure to estimate lifetimes of power devices in an IGBT module [17].

In the first step, loss profiles of power devices are obtained from input data such as device characteristics, converter characteristics, and mission profiles of power converter applications. Then, the loss profiles of power devices are converted to temperature profiles by thermal models of power devices. In step 3, the different temperature stress factors such as junction temperature swing (ΔT_j) and mean junction temperatures (T_{jm}) are counted from the temperature profiles by using a Rainflow

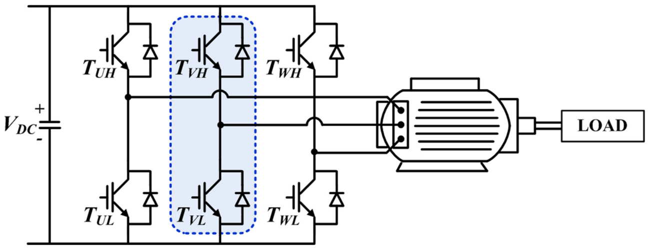

Fig. 5. Configuration of the three-phase motor drive system with PMSM for the case study.

TABLE I
PARAMETERS OF THE PMSM FOR THE CASE STUDY

Parameters	Symbol	Value	Unit
Nominal Power	P_n	5000	[W]
Nominal Torque	T_n	24	[Nm]
Nominal Speed	n_n	2000	[rpm]
Maximum Current	I_{max}	100	[A]
Maximum EMF	$V_{EMF,max}$	520	[V]
Rotor Inertia	J	0.0055	[Kgm^2]
Number of Pole pairs	N_{PP}	4	[-]
Stator Resistance	R_s	0.39	[Ω]
Stator Inductance	L_s	4.9	[mH]
DC-link Voltage	V_{DC}	400	V
Switching Frequency	f_{SW}	15	kHz

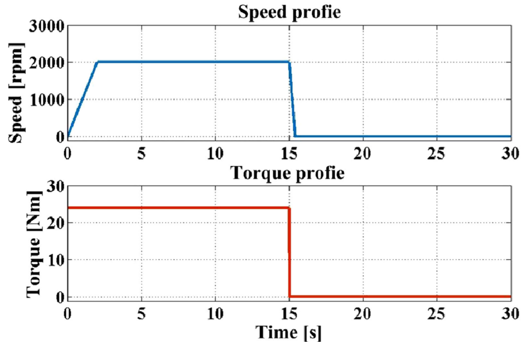

Fig. 6. Mission profile of the motor driver for the case study.

counting method [18]. Finally, lifetimes of power devices in the IGBT module are predicted based on a linear damage accumulation (LDA) rule by putting the accounted temperature stress factors into a lifetime model, which are typically developed by power cycling tests.

A. Motor Drive System

Fig. 5 shows a configuration of a three-phase motor drive system with a permanent magnet synchronous motor (PMSM) for the case study, and related parameters for the motor drive inverter and PMSM are listed in Table I.

Fig. 6 shows a mission profile composed of information on torque and speed profiles. The maximum torque is 24 Nm and the maximum speed is 2000 r/min. The motor is operated for 15 s with the maximum torque and the maximum speed with 2 s ramp-up time and then it is stopped for 15 s. Thus, the one period of the mission profile is 30 s. This is one of the typical start-run-stop processes in motor drive applications. The corresponding output currents and reference voltages of the motor drive under the given mission profile are shown in Fig. 7.

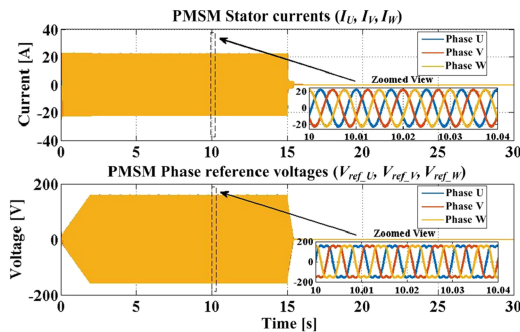

Fig. 7. Output currents and reference voltages under the given mission profile described in Fig. 6.

B. Power Loss Profiles

In order to get the thermal loadings of T_{VH} and T_{VL}, the power loss profiles of T_{VH} and T_{VL} should be obtained first.

The total power loss of the IGBT is composed of a conduction loss (P_{cond}) and a switching loss (P_{sw}).

The average conduction loss in one switching cycle can be represented as

$$P_{\mathrm{cond}(T_H/T_L)} = V_{\mathrm{CE_ON}(T_H/T_L)} \cdot I \cdot d \tag{1}$$

where I is the collector current, d is the duty cycle, and $V_{\mathrm{CE_ON}(T_H/T_L)}$ is the ON-state collector–emitter voltage at the certain reference junction temperature T_H or T_L.

The switching loss of the IGBT is calculated as

$$P_{\mathrm{sw}(T_H/T_L)} = f_{\mathrm{sw}} \cdot E_{\mathrm{sw}} \tag{2}$$

where f_{sw} is the switching frequency and E_{sw} is the switching energy of the IGBT at the certain reference junction temperature T_H or T_L.

Fig. 8 shows $V_{\mathrm{CE_ON}}$ and E_{sw} of the IGBTs when the junction temperatures are 125 °C (T_H) and 25 °C (T_L), respectively. Those values can be found in the datasheet or by experiments.

It is known that both switching and conduction losses are dependent on junction temperature, and thus, junction temperature information of power devices should be included when power losses are calculated.

Consequently, the conduction loss and the switching loss of the IGBT at the certain junction temperature can be computed as

$$P_{\mathrm{cond/sw}(T_j)} = \frac{P_{\mathrm{cond/sw}(T_H)} - P_{\mathrm{cond/sw}(T_L)}}{T_H - T_L}(T_j - T_L) + P_{\mathrm{cond/sw}(T_L)}. \tag{3}$$

Fig. 9 shows the loss profiles of T_{VH} and T_{VL} under the given mission profile shown in Fig. 6.

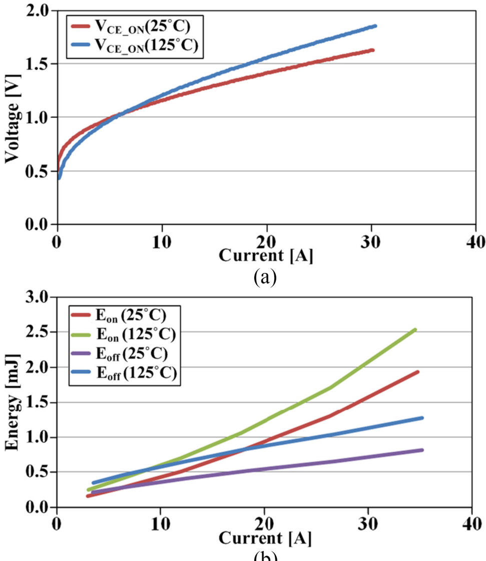

Fig. 8. $V_{\text{CE_ON}}$ and E_{sw} of the IGBTs when the junction temperatures are 125 °C (T_H) and 25 °C (T_L).

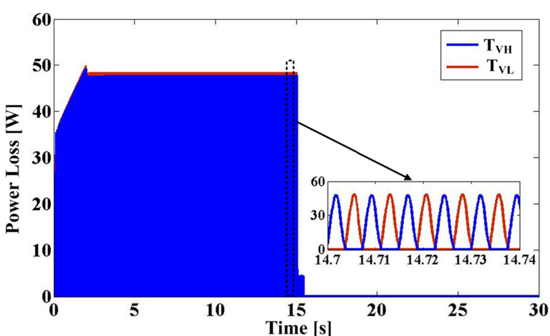

Fig. 9. Power loss profiles of T_{VH} and T_{VL} during the given mission profile (see Fig. 6).

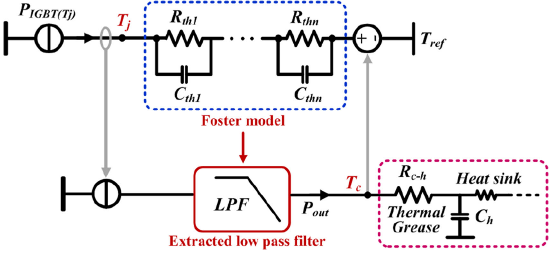

Fig. 10. Thermal impedance model for obtaining thermal loadings of the IGBTs [19].

C. Thermal Profile and Lifetime Estimation

The thermal loading of each device can be obtained from the power loss profiles and a thermal model with thermal impedances. In this paper, the thermal model proposed in [19] is used, as shown in Fig. 10, in order to translate the power loss profiles into the thermal loadings of the devices. This thermal model has two thermal paths.

The first thermal path is used for the junction temperature estimation. In this path, the multilayer *RC* Foster thermal network

TABLE II
JUNCTION TO CASE, CASE TO HEAT-SINK, AND HEAT-SINK TO AMBIENT THERMAL IMPEDANCES

Impedance	IGBT		i = 1	2	3	4
$Z_{th(j\text{-}c)}$ (Junction to case)	T_{VH}	R	0.6667	0.4060	0.3720	0.0801
		C	0.2419	0.0583	1.3502	0.0162
	T_{VL}	R	0.4221	0.8770	0.3717	0.0820
		C	1.1793	0.1937	0.0642	0.0170
$Z_{th(c\text{-}h)}$ (Case to heat-sink)	-	R	0.04132	-	-	-
		C	13.06	-	-	-

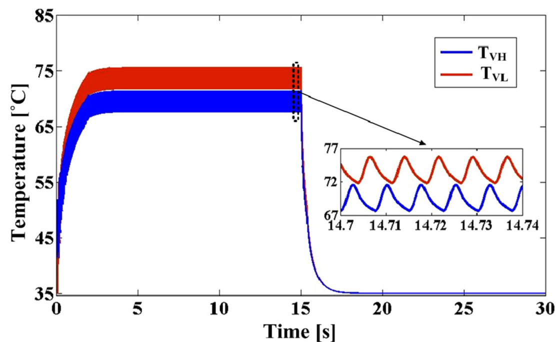

Fig. 11. Thermal loadings of T_{VH} and T_{VL} under the given mission profile of the motor drive system shown in Fig. 6.

is used. The *RC* Foster thermal network is represented as

$$Z_{\text{th}(j-c)}(t) = \sum_{i=1}^{n} R_i(1 - e^{-t/\tau_i}) \tag{4}$$

where $Z_{\text{th}(j-c)}$ is the junction to case thermal impedance, $\tau_i = R_i * C_i$, and i means the different layers of a power module for the Foster model. The related parameter can be obtained from datasheet or experiments. In this path, only the reference temperature (T_{ref}) is connected, where T_{ref} is determined by the case temperature T_c from the other thermal path.

The second thermal path is used for the temperature estimations outside the IGBT module such as case and heat-sink temperatures. In this path, the filtered power loss by a low-pass filter (LPF) is used to model the loss behaviors flowing out of the device, where the parameters for the LPF can be extracted from the *RC* Foster thermal network in the first thermal path. The filtered loss can help to obtain correct temperature behavior outside the IGBT module.

The thermal impedances of T_{VH} and T_{VL} and the related thermal impedances for this study are listed in Table II. In this simulation study, it is assumed that the heat-sink temperature is 35 °C.

Fig. 11 shows the thermal loadings of T_{VH} and T_{VL} under the given mission profile of the motor drive system. As expected in Section II-B, both IGBTs have almost the same junction temperature swing, which is less than 4 °C by the periodical commutation of the IGBTs with fast output frequency, as shown in the zoomed view of Fig. 11. However, they have different

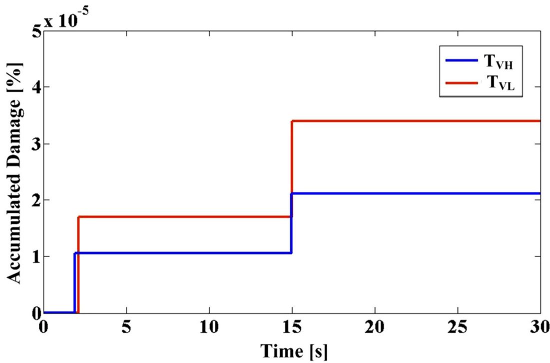

Fig. 12. Accumulated damages of T_{VH} and T_{VL} during a period of the mission profile based on the Semikron lifetime model.

thermal stresses in terms of junction temperature swing (ΔT_j) and mean junction temperature (T_{jm}) by the load variation. T_{VL} has a higher thermal loading compared to T_{VH}, and therefore, it can be expected that T_{VL} has a shorter lifetime than T_{VH}.

After the corresponding thermal loadings of T_{VH} and T_{VL} are obtained, the lifetimes of T_{VH} and T_{VL} can be estimated by mapping the thermal loadings to the lifetime model. The rainflow counting method is performed first in order to translate the thermal loading profiles of T_{VH} and T_{VL} into the number of cycles of different magnitudes of temperature stress factors such as ΔT_j and T_{jm} [16]. Then, the lifetimes are calculated based on the LDA rule [17], [20].

In the LDA rule, if there are k different stress levels and a certain material is exposed to a i_{th} stress for a certain number of cycles n_i and the number of cycles to failure at a i_{th} stress is N_i, a damage (D) can be represented as

$$D_i = \frac{n_i}{N_i} \tag{5}$$

where n_i is the number of cycles accumulated at i_{th} stress, and D_i is the damage of life consumed by exposure to the cycles at i_{th} stress level.

The total damage at different stress levels can be added up for a total accumulated damage (AD) as given in the following equation if different stress levels lead to the same failure mechanism:

$$AD = \sum_{i=1}^{k} \frac{n_i}{N_i} = \frac{n_1}{N_1} + \frac{n_2}{N_2} + \cdots + \frac{n_{k-1}}{N_{k-1}} + \frac{n_k}{N_k}. \tag{6}$$

Finally, failure occurs, when a total AD is reached to 1.

In this paper, the Semikron lifetime model presented in [15] is used since there is no existing lifetime model for the target IGBT module. Therefore, the lifetime value should be considered only for the purpose of the lifetime comparison between T_{VH} and T_{VL}.

Fig. 12 shows the AD of T_{VH} and T_{VL} based on the Semikron lifetime model during a period of the mission profile.

The lifetime can simply be calculated as follows:

$$\text{Lifetime} = \frac{\text{Period of mission profile (s)}}{\text{Operating time (s)} * \text{Accumulated damage}}. \tag{7}$$

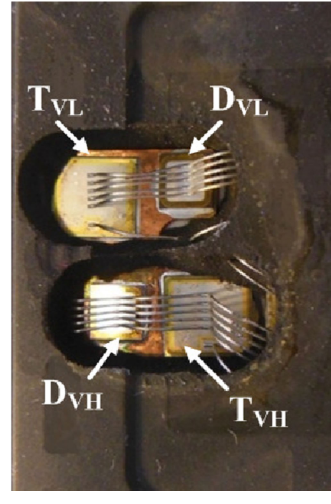

Fig. 13. Opened transfer molded IGBT module.

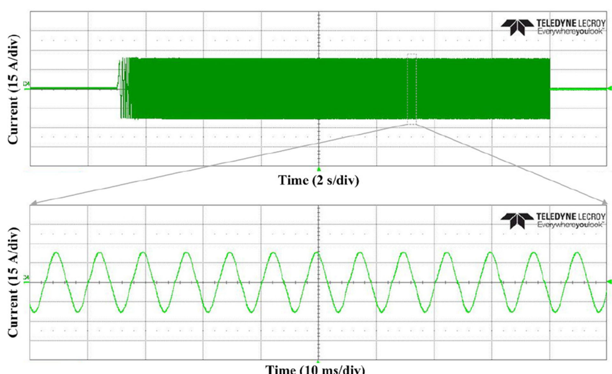

Fig. 14. Output current of phase-V during the given mission profile of the motor drive system.

If it is assumed that the motor system is operated for 12 hours per day, based on (7), the corresponding estimated lifetimes of T_{VH} and T_{VL} are about 9 and 5.6 years, respectively. The lifetime of T_{VL} is about 38% shorter than that of T_{VH}. In other words, the IGBTs in the lower group (T_{UL}, T_{VL}, T_{WL}) are the most reliability-critical devices, and thus, the lifetime of the inverter could depend on the lower group of IGBTs.

IV. Experimental Results

Experiments have been carried out in order to verify the effect of the asymmetric layout of IGBT modules on the reliability of motor drive inverters.

The same IGBT module with the simulation study, which is a 600 V, 30 A three-phase transfer molded IGBT module, has been used for the experiments. The IGBT module is opened, as shown in Fig. 13, and painted by black paint in order to measure junction temperatures of T_{VH} and T_{VL} by a high-resolution infrared camera (FLIR X8400sc) when it is operated under the given mission profile of the motor drive.

Fig. 14 shows the output current of the phase-V when the motor drive inverter is operated under the given mission profile, as shown in Fig. 6 and Table I. The heat-sink temperature is

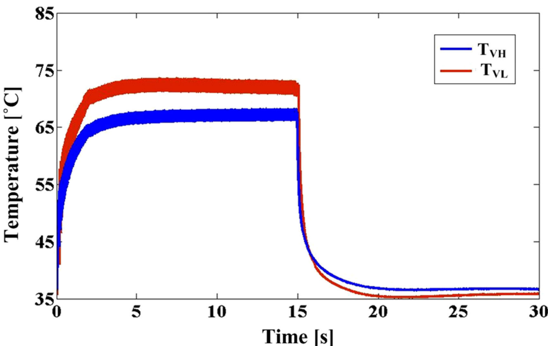

Fig. 15. Measured average junction temperatures of T_{VH} and T_{VL} by the infrared camera during the mission profile.

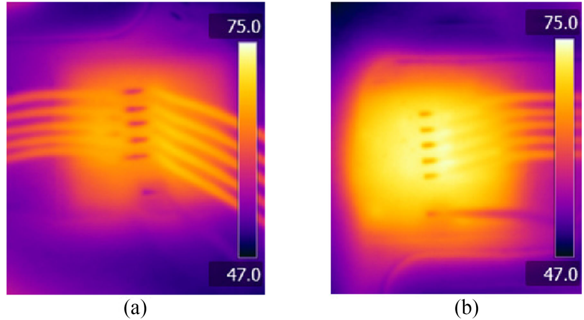

Fig. 16. Open transfer molded IGBT module taken by the infrared camera at the maximum temperature. (a) T_{VH}. (b) T_{VL}.

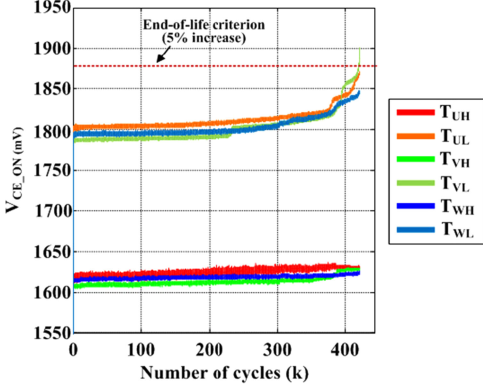

Fig. 17. Power cycling test result when output current $(I) = 29\ \mathrm{A_{peak}}$, output voltage $(V_{\mathrm{out}}) = 140\ \mathrm{V_{peak}}$, and output frequency $(f_{\mathrm{out}}) = 1$ Hz is applied.

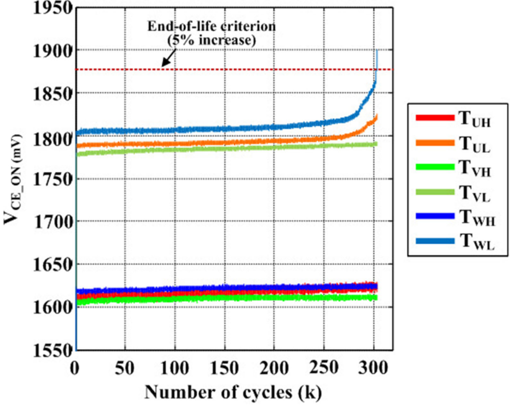

Fig. 18. Power cycling test result with another same type of the IGBT module under the same condition.

controlled by the water cooling system so that the average of the heat-sink temperature during the mission profile is kept about 35 °C.

Fig. 15 shows the average junction temperatures of T_{VH} and T_{VL} measured by an infrared camera under the given mission profile. The maximum average temperatures of T_{VL} and T_{VH} are about 73 and 68 °C, respectively. As expected, the thermal loading of T_{VL} is larger than that of T_{VH} in terms of junction temperature swing and the mean junction temperature due to the unbalance of the thermal impedance, which is caused by the internal asymmetric layout. Therefore, it can be expected that T_{VL} has a shorter lifetime than T_{VH}.

Fig. 16(a) and (b) shows the figures of T_{VH} and T_{VL} taken by the infrared camera when they have the maximum temperatures, respectively. It can be clearly seen that T_{VL} has a higher junction temperature than T_{VH}.

Furthermore, the power cycling test has been performed in order to verify that the IGBTs in the lower group (T_{UL}, T_{VL}, T_{VH}) have shorter lifetimes than the IGBTs in the upper group (T_{UL}, T_{VL}, T_{VH}). The power loading that output current $(I) = 29\ \mathrm{A_{peak}}$, output voltage $(V_{\mathrm{out}}) = 140\ \mathrm{V_{peak}}$, and output frequency $(f_{\mathrm{out}}) = 1$ Hz is applied to the IGBT module, where the heat-sink temperature is controlled as 25 °C. The reason that f_{out} is set to 1 Hz is to get the thermal loading in a second range easily by the output current and also to get the high thermal loading in order to get the test result in a reasonable testing time.

The end-of-life (EOL) criterion of the IGBT module is 5% increase of $V_{\mathrm{CE_ON}}$ from its initial value. $V_{\mathrm{CE_ON}}$ of the six IGBTs are measured in real-time per temperature cycle when the current is $\pm 20\ \mathrm{A_{peak}}$. More detailed information on power cycling test can be obtained in [10] and [21].

Fig. 17 shows the power cycling test result of the IGBT module. As expected, $V_{\mathrm{CE_ON}}$ of the IGBTs in the lower group (T_{UL}, T_{VL}, T_{WL}) increases earlier where $V_{\mathrm{CE_ON}}$ of T_{VL} is reached to the EOL criterion first at about 420 800 cycles. It can also be expected that the other lower IGBTs will be reached to EOL criterion soon. However, in the case of the IGBTs in the upper group (T_{UH}, T_{VH}, T_{WH}), there are not any visible increases in $V_{\mathrm{CE_ON}}$.

The power cycling test with another 600 V, 30 A three-phase transfer molded IGBT module also has been performed under the same condition, as shown in Fig. 18. $V_{\mathrm{CE_ON}}$ of T_{WL} is reached to the EOL criterion first at about 303 527 cycles and it is also expected that $V_{\mathrm{CE_ON}}$ of T_{UL} will increase to the EOL criterion. On the other hand, the increases in $V_{\mathrm{CE_ON}}$ of the upper IGBTs (T_{UH}, T_{VH}, T_{WH}) are not observed during the power cycling test.

These two test results clearly show that the IGBTs in the upper group (T_{UH}, T_{VH}, T_{WH}) have longer lifetimes than the IGBTs in the lower group (T_{UL}, T_{VL}, T_{WL}) because the lower

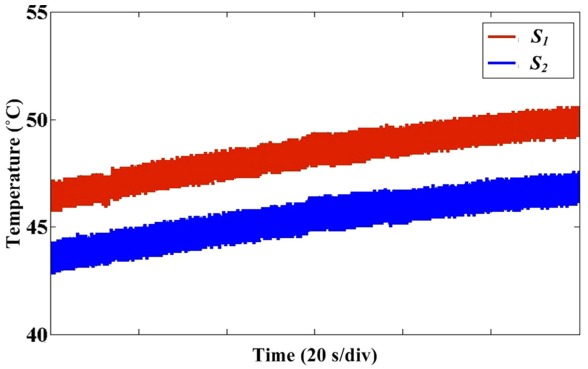

Fig. 19. Measured average junction temperatures of S_1 and S_2 by the infrared camera under the MMC operation.

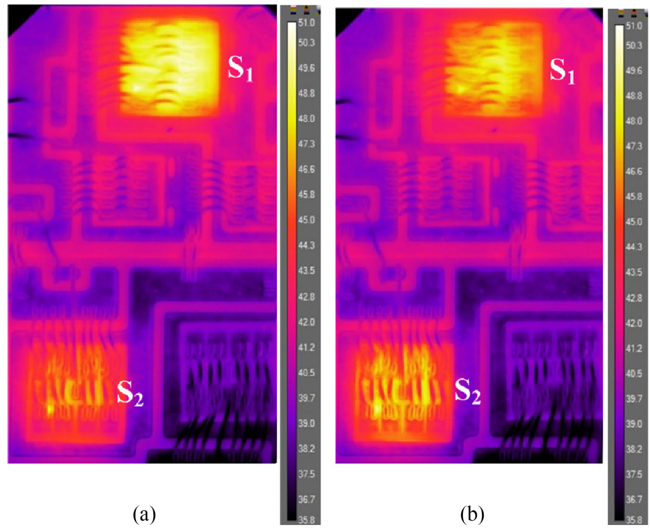

Fig. 20. Open full-bridge IGBT module taken by the infrared camera at the maximum temperature. (a) Upper IGBT S_1. (b) Lower IGBT S_2.

IGBTs have higher thermal loadings than the upper IGBTs due to the differences of the thermal impedances.

It is worth to mention that the initial $V_{\mathrm{CE_ON}}$ of the lower IGBTs are higher than those of the upper IGBTs. This is because the lower IGBTs have the higher internal resistance due to a longer current path in this module and also higher junction temperature at the point of $V_{\mathrm{CE_ON}}$ measurement due to the different thermal impedances between the upper and lower IGBTs.

More detailed information on the internal resistance of the target IGBT module can be obtained in [22].

Furthermore, the effect of the asymmetric layout of another type of IGBT module on the reliability of inverters has been validated with a small-scaled modular multilevel converter (MMC). A full-bridge IGBT module manufactured by Infineon (F4-50R12KS4) is used for a submodule of the MMC. Junction temperatures of upper and lower IGBTs of one leg in the full-bridge IGBT module are measured. In this paper, the submodule of the MMC is operated under the following conditions; dc-link voltage (V_{dc}): 100 V, output current $(I) = 40\ \mathrm{A_{peak}}$, modulation index $= 0.8$, switching frequency $(f_{\mathrm{sw}}) = 2$ kHz, and output frequency $(f_{\mathrm{out}}) = 50$ Hz. The upper IGBT is represented as S_1 and the lower IGBT is denoted as S_2.

Fig. 19 shows the average junction temperatures of S_1 and S_2 measured by the infrared camera for 120 s. The junction temperatures of S_1 and S_2 increase continuously because the heat-sink temperature is not under the steady-state condition. However, it can be clearly seen that S_1 has a higher junction temperature than S_2 due to the different thermal impedances caused by the asymmetric layout of the IGBT module. Therefore, they have the different thermal loadings in real applications, and thus, it can be expected that S_1 has a shorter lifetime than S_2.

Fig. 20(a) and (b) shows the figures of S_1 and S_2 taken by the infrared camera when they have the maximum temperatures, respectively. It can be clearly seen that S_1 has a higher junction temperature than S_2.

V. Conclusion

In this paper, an effect of asymmetric layout of IGBT modules on the reliability of power inverters has been studied. This study has been performed with 600 V, 30 A, three-phase molded IGBT modules under the three-phase motor drive application.

Due to the asymmetric internal layout of the IGBT module, the six IGBTs have the different thermal impedances and especially the lower IGBTs have higher thermal impedances than the upper IGBTs. Because of this, the IGBTs have the different thermal loadings under the given mission profiles of the motor drive application and finally lead to mismatched lifetimes. The lifetime of T_{VL} is shorter about 38%, which is 5.6 years than that of T_{VH}, which is 9 years. Consequently, the lower IGBTs ($T_{\mathrm{UL}}, T_{\mathrm{VL}}, T_{\mathrm{VH}}$) are the most reliability-critical devices. Thus, the lifetime and the power rating of the inverter may be limited by the lower group of the IGBTs. However, generally common data are provided for all devices in datasheet, and this may cause improper design of the inverter in terms of the lifetime and the power rating.

This effect has been verified by the experiments. As expected, the lower IGBTs have higher thermal loadings than the upper IGBTs and therefore have shorter lifetimes.

Furthermore, this effect has also been validated with the full-bridge IGBT module in the submodule of the small-scaled MMC. Due to the asymmetric layout of the IGBT module, the upper and lower IGBTs in one leg also have different junction temperatures. From the above-mentioned result, it can be expected that other kinds of IGBT modules can have an asymmetric internal layout, and therefore, they can affect the reliability of inverters for other different power electronic applications such as photovoltaic (PV) inverter, wind turbine converter, electric vehicle, and so on.

This study can provide a feedback to module designers on optimizing module's internal geometry such as a layout of a DBC so that power devices in power modules have thermal impedances as similar as possible for even lifetime distributions. Furthermore, it can also give suggestions for application engineers when the inverter is designed with the target lifetime and the power rating.

References

[1] P. Davari, Y. Yang, F. Zare, and F. Blaabjerg, "Multipulse pattern modulation scheme for harmonic mitigation in three-phase multimotor drives," *IEEE J. Emerging Sel. Top. Power Electron.*, vol. 4, no. 1, pp. 174–185, Mar. 2016.

[2] I. Boldea, "Electric generators and motors: An overview," *CES Trans. Electr. Mach. Syst.*, vol. 1, no. 1, pp. 3–14, Mar. 2017.

[3] K. J. P. Mackent, I. T. Wallace, and M. H. J. Bolleno, "Reliability assessment of motor drives," in *Proc. 37th IEEE Power Electron. Spec. Conf.*, Jun. 2006, pp. 1–7.

[4] S. Yang, A. Bryant, P. Mawby, D. Xiang, L. Ran, and P. Tavner, "An industry-based survey of reliability in power electronic converters," *IEEE Trans. Ind. Appl.*, vol. 47, no. 3, pp. 1441–1451, May/Jun. 2011.

[5] U. M. Choi, F. Blaabjerg, S. Jørgensen, S. Munk-Nielsen, and B. Rannestad, "Reliability improvement of power converters by means of condition monitoring of IGBT modules," *IEEE Trans. Power Electron.*, vol. 32, no. 10, pp. 7990–7997, Oct. 2017.

[6] W. Zhang, D. Xu, P. N. Enjeti, H. Li, J. T. Hawke, and H. S. Krishnamoorthy, "Survey on fault-tolerant techniques for power electronic converters," *IEEE Trans. Power Electron.*, vol. 29, no. 12, pp. 6319–6331, Dec. 2014.

[7] U. M. Choi, F. Blaabjerg, and K. B. Lee, "Reliability improvement of a T-type three-level inverter with fault-tolerant control strategy," *IEEE Trans. Power Electron.*, vol. 30, no. 5, pp. 2660–2673, May 2015.

[8] B. A. Welchko, T. A. Lipo, T. M. Jahns, and S. E. Schulz, "Fault tolerant three-phase ac motor drive topologies: A comparison of features, cost, and limitations," *IEEE Trans. Power Electron.*, vol. 19, no. 4, pp. 1108–1116, Jul. 2004.

[9] U. M. Choi *et al.*, "Power cycling test and failure analysis of molded intelligent power IGBT module under different temperature swing durations," *Microelectron. Rel.*, vol. 64, pp. 403–408, Sep. 2016.

[10] U. M. Choi, F. Blaabjerg, and S. Jørgensen, "Power cycling test methods for reliability assessment of power device modules in respect to temperature stress," *IEEE Trans. Power Electron.*, vol. 33, no. 3, pp. 2531–2551, Mar. 2018.

[11] K. Ma, H. Wang, and F. Blaabjerg, "New approaches to reliability assessment: Using physics-of-failure for prediction and design in power electronics systems," *IEEE Power Electron. Mag.*, vol. 3, no. 4, pp. 28–41, Dec. 2016.

[12] D. Zhou, H. Wang, and F. Blaabjerg, "Mission profile based system-level reliability analysis of dc/dc converters for a backup power application," *IEEE Trans. Power Electron.*, early access article, doi: 10.1109/TPEL.2017.2769161

[13] A. Volke and M. Hornkamp, *IGBT Modules - Technologies, Driver and Application*. Munich, Germany: Infineon Technol. AG, 2011. ISBN: 978-3-00-032076-7.

[14] M. Ciappa, "Selected failure mechanism of modern power modules," *Microelectron. Rel.*, vol. 42, nos. 4–5, pp. 653–667, Apr./May 2002.

[15] A. Wintrich, U. Nicolai, W. Tursky, and T. Reimann, *Application Manual Power Semiconductors*. Nuremberg, Germany: SEMIKRON Int. GmbH, 2011. ISBN: 978-3-938843-66-6.

[16] Y. Wang, K. Yamaguchi, K. Watabe, T. Tanaka, M. Rogers, and E. R. Motto, "A new multi-functional compact IPM for low power industrial application," in *Proc. IEEE Appl. Power Electron. Conf. Expo.*, Mar. 2017, pp. 3072–3075.

[17] U. M. Choi, K. Ma, and F. Blaabjerg, "Validation of lifetime prediction of IGBT modules based on linear damage accumulation by means of superimposed power cycling tests," *IEEE Trans. Ind. Electron.*, vol. 65, no. 4, pp. 3520–3529, Apr. 2018.

[18] L. R. GopiReddy, L. M. Tolbert, B. Ozpineci, and J. O. P. Pinto, "Rainflow algorithm-based lifetime estimation of power semiconductors in utility applications," *IEEE Trans. Ind. Appl.*, vol. 51, no. 4, pp. 3368–3375, Jul./Aug. 2015.

[19] K. Ma, N. He, M. Liserre, and F. Blaabjerg, "Frequency-domain thermal modeling and characterization of power semiconductor devices," *IEEE Trans. Power Electron.*, vol. 31, no. 10, pp. 7183–7193, Oct. 2016.

[20] J. A. Bannantine, J. J. Comer, and J. L. Handrock, *Fundamentals of Metal Fatigue Analysis*. Englewood Cliffs, NJ, USA: Prentice-Hall, 1990.

[21] U. M. Choi, S. Jørgensen, and F. Blaabjerg, "Advanced accelerated power cycling test for reliability investigation of power device modules," *IEEE Trans. Power Electron.*, vol. 31, no. 12, pp. 8371–8386, Dec. 2016.

[22] U. M. Choi, F. Blaabjerg, F. Iannuzzo, and S. Jørgensen, "Junction temperature estimation method for a 600 V, 30A IGBT module during converter operation," *Microelectron. Rel.*, vol. 55, nos. 9–10, pp. 2022–2026, Aug./Sep. 2015.

Ui-Min Choi (S'11–M'16) received the B.S. and M.S. degrees from Ajou University, Suwon, South Korea, in 2011 and 2013, respectively, and the Ph.D. degree from Aalborg University, Aalborg, Denmark, in 2016, all in electrical engineering.

From 2016 to 2018, he was with the Department of Energy Technology, Aalborg University, as a Post-Doctoral Researcher. In 2018, he joined the Department of Electronic and IT Media Engineering, Seoul National University of Science and Technology, Seoul, South Korea, where he is currently an Assistant Professor. He was a Partner Researcher with Grundfos Holidng A/S, from 2014 to 2016. His research interests include reliability of power device and power converter systems, renewable energy generation, and multilevel converter.

Dr. Choi received the IEEE Transactions on Power Electronic Second Prize Paper Award in 2017.

Ionut Vernica (S'17–M'17) was born in Romania, in 1992. He received the B.Sc. degree in electrical engineering from the Politehnica University of Bucharest, Bucharest, Romania, in 2014, and the M.Sc. degree in power electronics and drives from Aalborg University, Aalborg, Denmark, in 2016.

Since July 2016, he has been with the Department of Energy Technology, Aalborg University, where he is currently a Research Assistant. His current research interests include control of adjustable speed drives, thermal management of power devices, emerging power electronics applications, and the reliability of IGBT power modules and capacitors.

Frede Blaabjerg (S'86–M'88–SM'97–F'03) received the Ph.D. degree in electrical engineering from Aalborg University, Aalborg, Denmark, in 1992.

He was with ABB-Scandia, Randers, from 1987 to 1988. He became an Assistant Professor in 1992, an Associate Professor in 1996, and a Full Professor in power electronics and drives in 1998. From 2017, he became a Villum Investigator. He has authored or coauthored more than 500 journal papers in the fields of power electronics and its applications. He is the coauthor of two monographs and the editor of seven books in power electronics and its applications. His current research interests include power electronics and its applications such as in wind turbines, PV systems, reliability, harmonics, and adjustable speed drives.

Dr. Blaabjerg was the Editor-in-Chief for the IEEE TRANSACTIONS ON POWER ELECTRONICS from 2006 to 2012. He was a Distinguished Lecturer for the IEEE Power Electronics Society from 2005 to 2007 and for the IEEE Industry Applications Society from 2010 to 2011 as well as 2017 to 2018. In 2018, he is the President Elect of the IEEE Power Electronics Society. He received 24 IEEE Prize Paper Awards, the IEEE PELS Distinguished Service Award in 2009, the EPE-PEMC Council Award in 2010, the IEEE William E. Newell Power Electronics Award 2014, and the Villum Kann Rasmussen Research Award 2014. He was nominated in 2014–2017 by Thomson Reuters to be among the most 250 cited researchers in Engineering in the world. In 2017, he became Honoris Causa at the University Politehnica Timisoara, Timisoara, Romania.